IEEE Journal of Translational Engineering in Health and Medicine

Received 21 June 2017; revised 23 August 2017 and 6 September 2017; accepted 14 September 2017.
Date of publication 20 October 2017; date of current version 18 December 2017.

Digital Object Identifier 10.1109/JTEHM.2017.2761873

Developing a Wireless, High Precision and Processing Speed Pulse Monitoring Headset Using Photoplethysmography

YUNHUI JIANG[1], JIAN TANG[1], XIAOLIANG WANG[2], AND CHAO SHEN[1]

[1]Yancheng Teachers University, Yancheng 224002, China
[2]Institute of Semiconductors, Chinese Academy of Sciences, Beijing 100864, China

CORRESPONDING AUTHOR: J. Tang (jtang1982@163.com)

This work was supported in part by the National Key Research and Development Program of China under Grant 2016YFB0400104 and Grant 2016YFB0400301 and in part by the National Nature Sciences Foundation of China under Grant 61334002.

ABSTRACT In this paper, thorough improvement of pulse monitoring and analysis equipment with a headset structure is presented. In order to study the most suitable infrared wavelength for the acquisition of the pulse wave at the earlobe, Monte Carlo simulation was adapted. Both high frequency noise and baseline drift, generated in the signal acquisition process, are considered. To further optimize the system design and improve accuracy, for the sensor's dimensional drift, the corresponding compensation was carried on in the software. This paper introduced nonlinear quantization, especially in terms of very weak pulse signal, in the time domain analysis process. A quick extraction method named table look-up combing with interpolation was utilized to obtain frequency domain information whose processing speed can be increased by about 30 times compared with fast Fourier transformation setting the sampling point as 300. The results demonstrated the sensor's excellent performance in pulse signal acquisition whose maximum residual is less than 0.004 mV. The test on a random sample of 300 people indicates that the system had high correlation with reference, validating the system accuracy is extremely high. Overall, this paper provides a practical pulse monitoring and analysis system with high precision and processing speed that can be widely applied in the field of health management or medical measurement.

INDEX TERMS Monte Carlo simulation, earlobe pulse, time - frequency analysis, non-linear quantification, temperature compensation.

I. INTRODUCTION

Pulse wave becomes a hot spot of research nowadays for the finding can show a significant pathway linking to cardiovascular diseases [1]. The propagation characteristics of pulse wave go hand in hand with the variety of the cardiovascular system parameters. For instance, the pulse wave velocity (PWV) depending on period can be used to evaluate the regional arterial stiffness [2], [3]. Pulse wave monitoring, extraction and analysis have great significance for early detection of health issue and clinical treatment. In theory, the relationship between pulse wave and cardiovascular blood flow dynamics is established which lays the foundation of developing noninvasive and efficient medical instruments. So far, a variety of instruments have been developed and produced [4], [5]. In particular, with the prevalence of wearable devices, 24-hour health dynamic monitoring technology is maturing. As an affordable, wearable physiological measurement, wrist-type heart-rate tracker becomes one of the most typical devices [6], [7]. But because of human movement interference and constraints of sensor technology, exact heart rate extraction from pulse wave during intensive physical activities remains challenging, let alone other physiological information.

As early as 2002, Jeon *et al.* have put forward a method to collect the different wavelengths of the photoelectric volume pulse wave using five wavelengths of the LED array as the light source. The calculation of hemoglobin concentration and wavelength selection was studied as well [8]. The

pulse wave spectrum of finger transmission was obtained by Yamakoshi *et al.* [9] using the high-speed acquisition system of 900∼1700nm near-infrared spectroscopy. The blood glucose prediction model established by partial least squares regression (PLS) was used to predict the blood glucose of 22 and the precision can reach 22.3 mg / dL (1.23 mmol / L). Nitzan and Engelberg [10] proposed a method of measuring arterial oxygen saturation through three adjacent wavelengths, taking the effects of scattering into account in principle. Besides that, it did not need correction, but the method lacked of experimental validation. As a general view, portability, multi-environment using, system accuracy and speed are still the obstacles to the development. High frequency and motion artifacts are among the leading causes of deviation in the progress of the acquisition of signals. The back-end processing circuit face a certain challenge in the aspect of processing speed and system accuracy. Our system detection parameters are relatively limited, which is one of the key points in our future research improvement. Of course, for some special scenes, we hope to achieve non-touch human health monitoring.

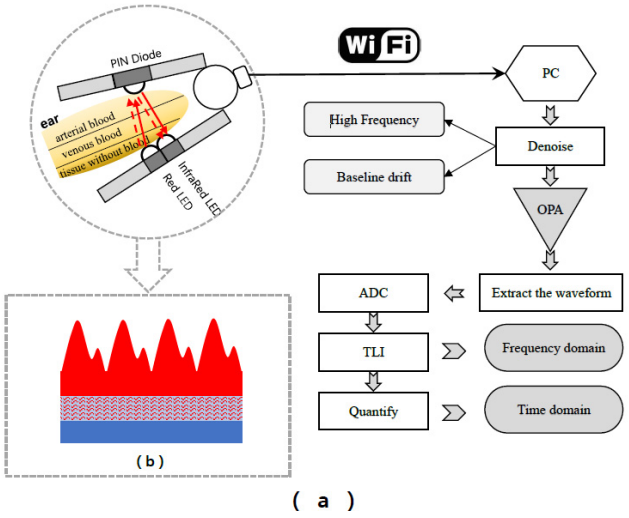

FIGURE 1. **The theoretic framework of the developed design.**

In this work, a wireless high precision and processing efficiency pulse instrument is designed which can match from minus 18° to 41° above zero. Overall design contains three parts: signal acquisition, pre-processing and information extraction. Using Lambert-Beer theorem set as a starting point [11], most photoelectricity pulse wave instruments have a common disadvantage, which is the scattering effect of human tissue and blood is ignored and only focuses on absorption effect. Firstly, Monte Carlo method is used in the acquisition part of the signal, aiming to screen out optimal test wavelength. What has been shown in Fig.1(b) is the intensity results extracted by single shot. Different optical adsorption properties of different human tissue can be clearly identified, with particular features of the plots explored using 630nm as an example. The result is plotted in Fig.2(a). Dynamic spectrum theory suggests that the light absorption of the muscles, subcutaneous fat, intravenous and other static tissue in earlobes as well as the basic absorption of the arteries all keep constant, the only change in absorbance changes is in the blood of the periodic pulsation part. When the arterial filling reaches the highest and the blood vessels are filled with blood, the transmittance of the earlobe reaches the minimum ($I_{\min}$). In a similar way, when the arterial filling reaches the lowest, the transmitted light will be up to the strongest ($I_{\max}$) [12]. In addition, the result of pulsating arterial blood absorbing light over time can be found clearly. In the second part, an algorithm with a capability of filtering high frequency noise and baseline drift at the same time has been studied which can extremely enhance the processing velocity and a standard signal will be obtained in order to follow-up use. Last but not least, for analyzing the models in time and frequency domain, nonlinear quantization and table look-up combining with interpolation has been put forward respectively.

II. METHODS

A. PULSE WAVE ACQUISITION

The first step in pulse quantification and analysis is to acquire the pulse wave signal via sensor system. The core task of the pulse wave acquisition module is to acquire pulse wave with sufficient quality and resolution, while the selected sensor indicator significantly influences the properties, quality, reliability and validity of a pulse analysis system. Issues having to take into account for the design of a sensor system are discussed in the following.

Pulse wave sensors based on infrared (IR) or red light signals with a photo detector become the preferred choice for non-invasive, portable and low-cost test [13]. The photoplethysmography (PPG) reflects blood movement in the vessel through the amount of the backscattered light corresponds with the variation of the blood volume which was first found by Hertzman in 1938 [14]. Intense researches on the basis of it can replace some methodology like the management of vascular disease especially the invasive tests [15]. The selection of source to detector as well as wavelength selection which directly impact photoplethysmogram (PPG) is a crucial step. Besides, propagation of the light through different tissues is distinct. The relation absorbance of oxygenated and deoxygenated hemoglobin decides the wavelength which is selected for further study [16]. In terms of selection of infrared wavelength of sensor, this work puts forward an improved simulation method taking both the particularity of organizational structure and the characteristics of the light source into consideration.

Monte Carlo modelling of photon propagation has been used to improve upon established models in respect of the processing of circuit and operational accuracy. As is shown in Fig.1, tissue can be divided into three parts: tissue without blood including skin, fat and bones; venous blood; arterial blood. Of the three, tissue without blood and venous blood

IEEE Journal of Translational Engineering in Health and Medicine

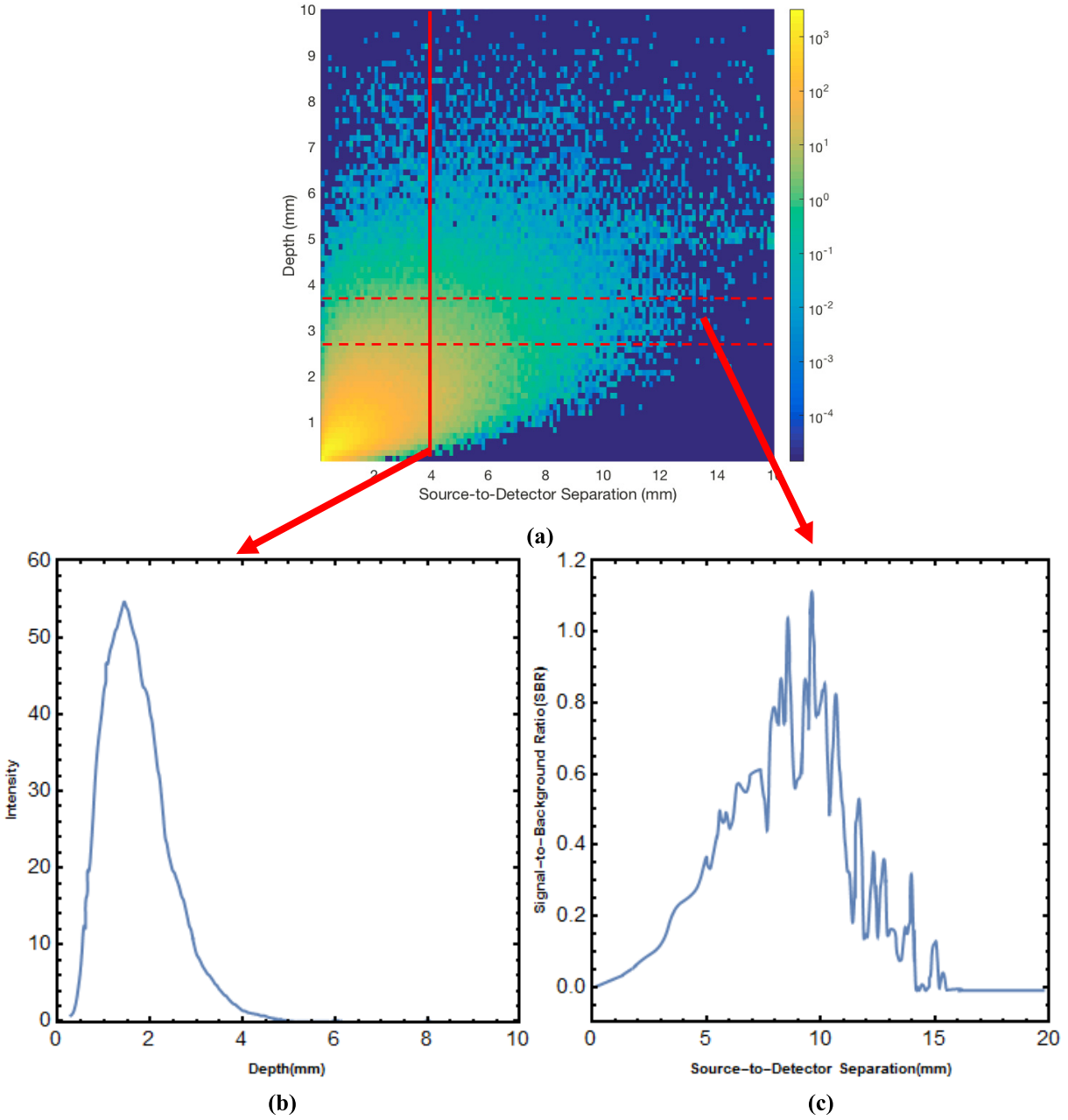

FIGURE 2. **Intensity of light exiting the tissue as a function of both source-to-detector separation and the depth reached by the photon for the wavelength(630 nm). (a) Intensity of light exiting the tissue. (b) Intensity at different depth (c) Radio at the particular separation.**

the intensity of the emitted light does not vary with the incident light intensity. Through research, the depth reached by the photon for the 660nm wavelength is shown in Fig.2(a). In Fig.2(c), the signal-to-background ratio is shown, with particular features using the depth from 2.6nm to 3.6nm as an example. This can be used to determine which source-to-detector separation is optimal for a particular probing depth. The intensity results extracted by single shot is plotted in Fig.2(b) while different optical adsorption properties of different human tissue can be clearly identified at 630nm, the probability distribution of reflection at 12.5 mm is plotted in Fig.3.

The equation used for Monte Carlo simulation gives as:

$$R(\alpha_i) = \frac{1}{2\sin^2(\alpha_i + \alpha_t)} + \frac{\tan^2(\alpha_i - \alpha_t)}{\tan^2(\alpha_i + \alpha_t)} \quad (1)$$

and the flow of the simulation process is shown below:

B. PULSE WAVE PRE-PROCESSING

To recognize the inflection points and easier interpretation of the original pulse wave, Takazawa *et al.* [17] introduced the first and the second derivative of the pulse signals, as shown in Fig.3. Furthermore, the second derivative is closely related to a selection of standard pulse wave which is the very

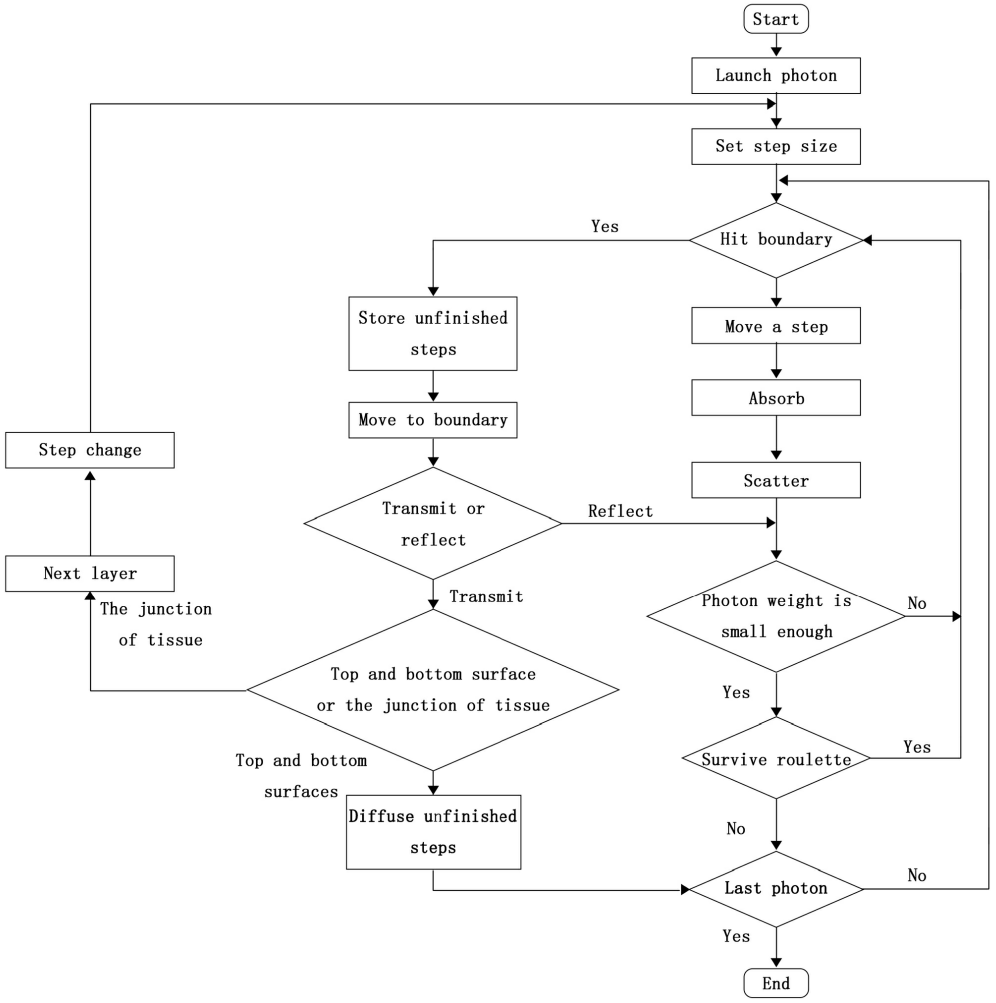

(a)

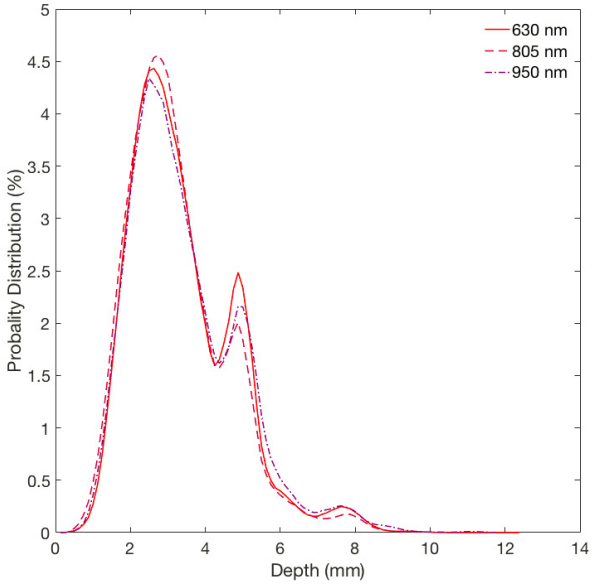

(b)

FIGURE 3. **Monte Carlo modeling. (a) The flow of the simulation process. (b) Probability distribution of reflection at 12.5 mm.**

IEEE Journal of Translational Engineering in Health and Medicine

foundation of further treatment. As the human pulse signal is relatively weak, different diversities of additive artifact inevitably generate, unfortunately affect the extraction of features [18]. Among the noise, high frequency noise which is the main influence factors is mostly caused by the instrument thermal noise and electromagnetic interference in the signal acquisition process [19]. Another main noise that influence the data processing is the baseline drift, especially occurs in the first started testing, which may lead to consequences like detect the peak value incorrectly. The main reason for the baseline drift is that the physical activity of testers, such as breathing and coughing, is low frequency noise. The original signal can just be able to discern while the first and the second derivative of the pulse signals is completely distorted. That is to say, the original pulse comes with a lot of noise need to be cleaned which will result in the serious distortion after the first and the second derivatives that affect subsequent processing. Therefore, filtering the high frequency noise and removing the baseline drift are both indispensable in the pre-processing.

1) ADD WHITE NOISE TO THE ORIGINAL SIGNAL

The original signal is defined as $X(t)$. First of all, white noise is added into it which is given as:

$$X'(t) = X(t) + c_i N_i(t) \tag{2}$$

where c_i is the amplitude of white noise. Then the empirical mode decomposition is applied in the signal decomposition. Repeat the above operation z times, where z generally opts for 100∼200. The signal can be represented as:

$$X'(t) = \sum_{i=1}^{n} IMF_i + r_n(t) \tag{3}$$

where i is an integer greater than or equal to 1 but equal to or less than n, $r_n(t)$ indicates the remainder. $IMF_1 \sim IMF_n$ are all the intrinsic mode function components from the decomposition. A sequence is given after space reconstruction (4), as shown at the bottom of the next page.

The parameter a in the sequence falls inside the range of $1 \le a \le N - (\alpha - 1)\lambda$. α indicates the embedded dimension while λ represents time delay.

2) CALCULATE THE PERMUTATION VALUE FOR EACH INTRINSIC MODE FUNCTION COMPONENT AND SELECT THE THRESHOLD

Permutation entropy is a method to detecting the randomness of time series and dynamic mutations. The vectors from $IMF_i(a)$ are sorted in ascending order, then all the components from the decomposition obtains a set of symbolic sequences $Sgn(j) = \{\beta_1, \beta_2, \cdots, \beta_n\}$, where j is an integer from 1 to a while a is less than or equal to $\alpha!$. The permutation entropy of the intrinsic mode function component from the decomposition can be given as:

$$PE_i(\alpha) = -\sum_{j=1}^{a} P_j \ln P_j \tag{5}$$

P_j expresses the probability of the occurrence of each symbol whose value equals $1/\alpha$ decides that $PE_i(\alpha)$ secures the maximum value ln $(\alpha!)$. After standardizing, the permutation entropy of the intrinsic mode function component from the decomposition $PE_i = PE_i(\alpha)/\ln\ (\alpha!)$ is finally obtained.

Another essential parameter needed to be defined is the threshold of the permutation entropy that is used to distinguish out high frequency noise $\{IMF_1, IMF_2, \cdots IMF_p\}(p \in$ Integer, $1 \le p \le n)$ and baseline drift components $\{IMF_h, IMF_{h+1}, \cdots IMF_p\}(h \in$ Integer, $1 \le p \le n)$.

3) GET THE STANDARD PULSE WAVE

Reconstructing signal is the last step of denoise processing, but the first step of further processing. The reconstructed signal is represented as the expression when baseline is given as $B = \sum_{k=h}^{n} IMF_k + r_n(t)$:

$$R(t) = \sum_{l=p}^{h} IMF_l + line(B(m)) \tag{6}$$

where k is an integer between h and n, $line(B(m))$ is the baseline after tanking the average of B. m is the number of sampling points and l is an integer in the range of m and n.

C. PULSE INFORMATION EXTRACTION

Sampling frequency f in the periodicity range of a human photovoltage pulse wave is between 0.3 and 2s, the number of sampling points in a human photovoltage pulse wave period is $0.3f \sim 2f$. Then the second sample sequence $R(t)$ is sampled by $\{C_{t'}\} == \{R_1, R_\tau, R_{2\tau}, R_{3\tau} \ldots\}$, where $\tau = 0.3f/100$. The filter window size is set at 70 points, the third sequence $Q_{t''}$ will get.

$$Q_{t''} = \frac{1}{20} \sum_{k'=0}^{k'=19} C_{x'+k'} \tag{7}$$

where k' is an integer; $C_{t'+k'}$ represents the sequence sample value of the $x' + k$ term.

Under circumstance of testing calmly, human pulse wave shows certain periodicity. In other words, the information content of it is just simple repetition that will result in both hardware and software waste. The ongoing study is based on a single cycle of the pulse signal. When the adjacent periodic error is not more than 98% and the cycle repeats more than five times, the last cycle is selected as the standard signal.

The second derivative of the sequence $R(t)$ is used in order to select the starting and ending points which are two extreme points on it. Define these two points as p_1 and p_2, then search the minimum value according to the sampling range defined before, the truncation range is ultimately ascertained. As is expected, truncated sequence $f(n')$ can be obtained (see Fig. 4).

Since the pulse wave is a nonlinear signal, a great deal signal rich in information is weak to detect but important in the analysis process. In order to address the current challenge, non-uniform quantification is suggested whose core is

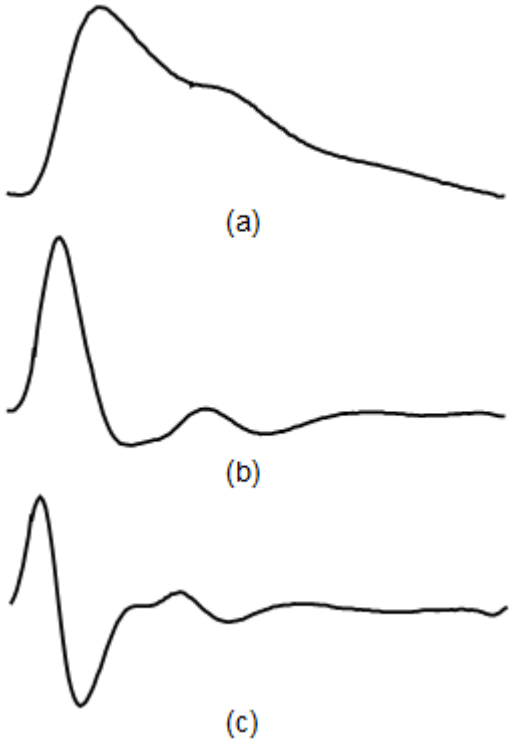

FIGURE 4. (a) Standard pulse wave; (b) Primary differential pulse wave; (c) Quadratic differential pulse wave.

enlarge the wake part of pulse wave and compress the large part. To visually view the process, Fig. 5 is plotted as below. The quantification function is given as:

$$y = \begin{cases} \dfrac{Ax}{1+\ln A}, & 0 \le x \le \dfrac{1}{A} \\ \dfrac{1+\ln(Ax)}{1+\ln A} & \dfrac{1}{A} \le x \le 1 \end{cases} \tag{8}$$

The meaning of parameter A is compressibility factor, directly affecting the compression effect. An additional impact is that the signal-noise ratio of the small signal can be significantly improved by this way.

After above-mentioned pre-processing of the original signal, a truncated sequence $f(n')$ including N sampling points is finally got. A new method named table look-up combing with interpolation (TLI) whose key steps are table look-up and interpolation has been introduced to reduce both computation time and register space.

$$\begin{aligned} T_{(n')} &= \sin(\frac{2\times(n'\%N)\pi}{N}) \\ T_{(n'+75)} &= \cos(\frac{2\times(n'\%N)\pi}{N}) \end{aligned} \tag{9}$$

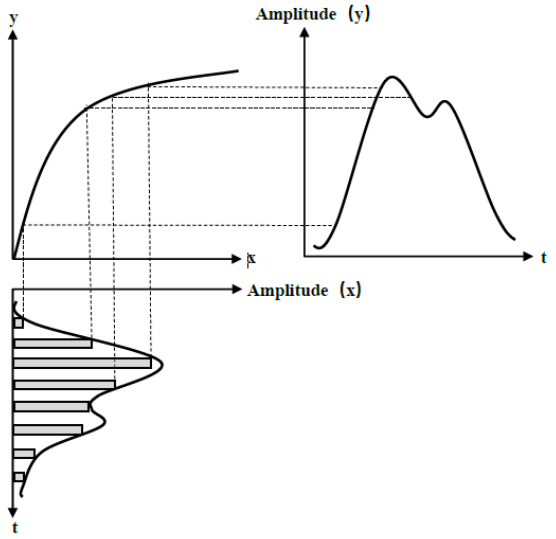

FIGURE 5. Pulse wave through non-uniform quantization.

The pulse wave function is substantially the result of interpolation from the truncated sequence $f(n')$, named $V(x)$.

$$V(x) = [f(b') - f(a')] * [\frac{N}{x}(l-1) + 1 - a'] + f(a') \tag{10}$$

where l is the length of sequence $f(n')$, $a' = \lfloor \frac{N}{x}(l-1)+1 \rfloor$, $b' = \lceil \frac{N}{x}(l-1)+1 \rceil$, $\lfloor\rfloor$ mea-ns rounding down and $\lceil\rceil$ means rounding up. $f(a')$ and $f(b')$ are both interpolation signals.

$$P_k^2 = (\frac{1}{\pi}\int_0^l f_{(n')} \sin\frac{2\pi kx}{l})^2 + (\frac{1}{\pi}\int_0^l f_{(n')} \cos\frac{2\pi kx}{l})^2 \tag{11}$$

where k is the power of harmonic component. Through table look-up, power components extract quickly.

$$\begin{aligned} P_k^2 = (\frac{1}{k\pi}\sum_{x=1}^{N} V_{(x)}(T_{(k(x-1)+75)} - T_{(kx+75)}))^2 \\ + (\frac{1}{k\pi}\sum_{x=1}^{N} V_{(x)}(T_{kx} - T_{kx-k}))^2 \end{aligned} \tag{12}$$

III. RESULTS

A. STANDARD WAVEFORM OUTPUT

As shown in Fig.6, (a) is the original wave with high frequency and baseline drift, which cannot be used for further processing. After the signal processing, as described

$$\left\{ \begin{array}{c} IMF_i(1) = \{IMF_i(1), IMF_i(1+\lambda), \cdots, IMF_i(1+(\alpha-1)\lambda)\} \\ IMF_i(a) = \{IMF_i(a), IMF_i(a+\lambda), \cdots, IMF_i(a+(\alpha-1)\lambda)\} \\ \vdots \\ IMF_i(N-(\alpha-1)\lambda) = \{IMF_i(N-(\alpha-1)\lambda), IMF_i(N-(\alpha-2)\lambda), \cdots, IMF_i(N)\lambda)\} \end{array} \right\} \tag{4}$$

IEEE Journal of Translational Engineering in Health and Medicine

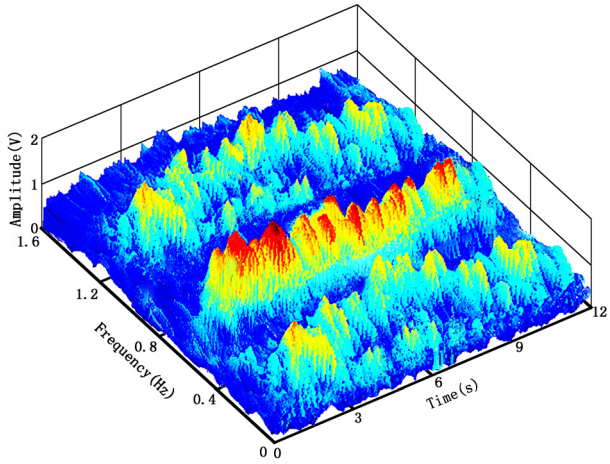

FIGURE 6. Spectrum plot of pulse wave.

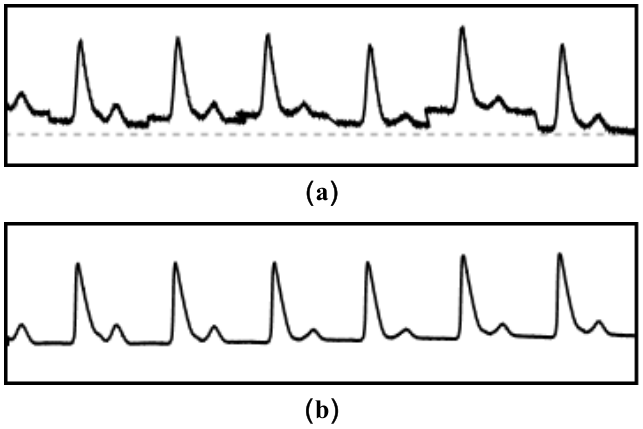

FIGURE 7. Pulse wave output. (a) Original wave with high frequency and baseline drift. (b) Preprocessed wave used for further processing.

in the part of pre-processing, standard waveform is plotted in Fig.6 (b). A residual analysis is used to identify predictors of the system accuracy through the extracted standard pulse signals after sampling and pre-progressing, the result of which is represented in Fig.7. As expected, maximum residual is less than 0.004mV.

B. MONITORING HEART RATE AND OXYGEN SATURATION OF DIFFERENT AGES REPEATEDLY

A typical single-cycle pulse wave is illustrated including abundant parameters [20]. On one hand, time domain analysis has the advantages on comprehending and interpreting straightly. On the other hand, time domain signals are however that occasionally, some components of pulse wave are weak and illegible, which cause a loss of information. Only when joint time-frequency analysis is taken, exact credibility will get. Besides, non-uniform quantification further increases the precision. In order to test the accuracy and efficiency of the system, test samples from different age classes has been selected randomly.

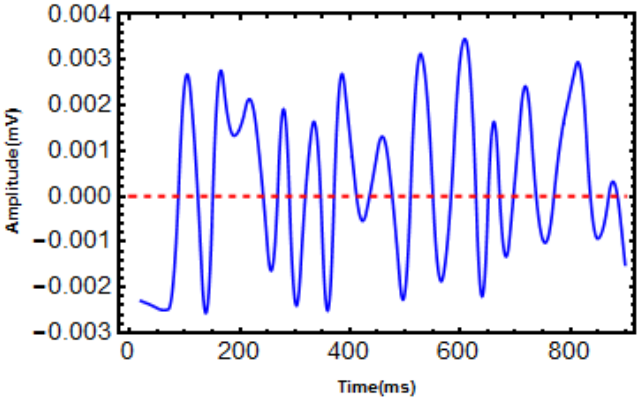

FIGURE 8. Residual analysis.

First, heart rate and oxygen saturation parameters have been tested and the results have been plotted as Fig.8. Testers are divided into three groups on the basis of age, each group of 30 people:

- Group "A": age from 10 to 35
- Group "B": age from 36 to 60
- Group "C": age from 60 to 80

The signal was collected in the tests' earlobe when they were in a calm state. The instrument acquires no imposed conditions on the test environment because the temperature compensation has been taken into account in the design process. To minimize the influence of accidental errors in the test, the test samples all tested three times.

Heart rate (HR) monitoring using photoplethysmography (PPG) has become a necessary feature in the wearable devices whose precision has been further optimized in this system.

$$HR = \frac{60 f_s}{N_T} \tag{13}$$

where f_s means the sampling frequency and N_T means the number of pulses in a single cycle.

Under normal conditions, heart rate is between 50 to 90 and it goes down slightly but not obviously with age. As expected, doing exercises is another factor affecting the heart rate. For example, supposing your resting heart rate begins to increase, you may exercise too hard or for too long.

Beyond that, oxygen saturation is also a parameter that must think over which is one of the important physiological parameters that characterizes human health.

Blood oxygen saturation test has been not only used to learn the health of the human cardiovascular and respiratory system, but also widely used in surgical anesthesia, patient first aid and neonatal care [21], [22]. Whether oxygen saturation is too low or drops rapidly will cause health threats, largely among the elderly. The system offers a reliable, non-invasive, convenient way for continuous monitoring of it. It can be seen from Fig.8(b) oxygen saturation is generally above 92%.

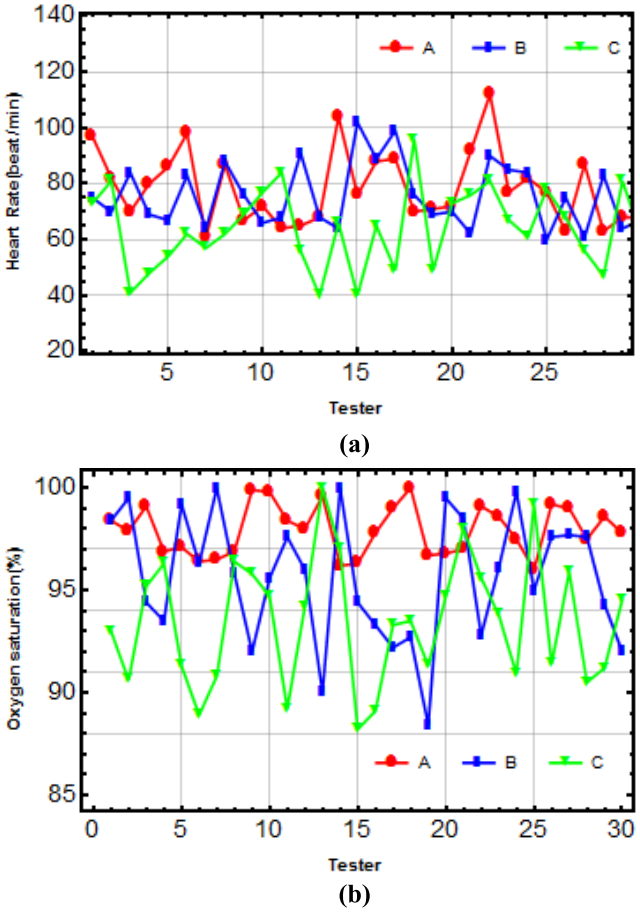

FIGURE 9. Basic parameter test results(Heart Rate and Oxygen Saturation). (a)The result of Heart Rate. (b)The result of Oxygen Saturation.

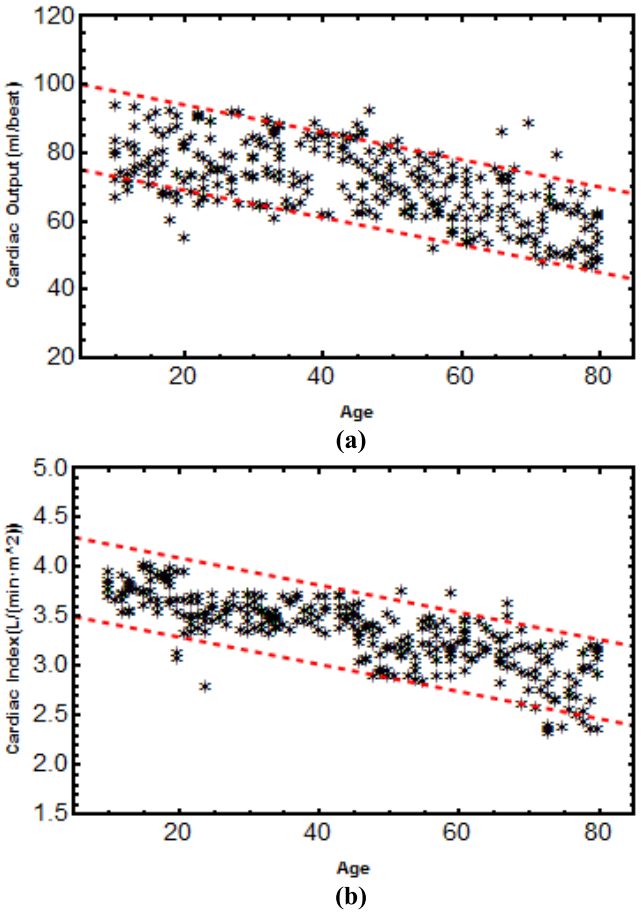

FIGURE 10. Expanding parameter test results(Cardiac Output and Cardiac Index). (a)The result of Cardiac Output. (a)The result of Cardiac Index.

C. CARDIAC OUTPUT AND CARDIAC INDEX MEASURED DURING REST

In the previous pulse instrument design, it was shown that detecting the heart rate and oxygen saturation is possible. Whereas the information contained in pulse wave is much more than this, cardiac output as well as cardiac index are also included in this system. In order to accurately study the reliability of the system, sample size increased to 300. The 300 volunteers, aged 9 to 82, are in different health condition. The median age of them is 42.7.

$$CO = \frac{17}{K^2}(P_s - P_d) \tag{14}$$

where P_s is systolic pressure, P_d is diastolic pressure, and K is given by $K = \frac{P_m - P_d}{P_s - P_d}$, P_m average pulse pressure.

$$CI = \frac{CO}{BSA} \tag{15}$$

where BSA is body surface area.

A series of two experiments for each test has been taken to limit the defected error and suppress the accidental error. The measurement results are shown in Fig.9.

Both cardiac output and cardiac index show a weakening trend with age (see Fig. 10). Cardiac output is key characteristics of the pumping force of the heart and cardiac index is closely bound up with it. In case both cardiac output or cardiac index are beyond normal values, it may mean that myocardial contractility is too high and you are suffering from high blood pressure. If continues, over time, oxygen consumption will increase and in serious cases it can cause myocardial damage and ultimately threaten the life. On the contrary, too low cardiac output and cardiac index can be the precursor for low blood pressure.

IV. DISCUSSION

Due to the characteristics of the photoelectric sensor, the measurement accuracy is affected by the temperature, resulting heavily but unallowable skew especially in the measurement of high precision. In order to improve the accuracy further, accurate and effective compensation is urgently needed. The hardware compensation is small and the accuracy is so low that cannot meet the reality requirement while a flexible, high precision and relatively low-cost compensation mode which is completely depend on the software. Further studies conclusively showed the photoelectric sensor performs

TABLE 1. Temperature Drift of the Sensor at Different Temperature

Test	Temperature (°C)	$Cold_{RMS}$ (V)	Temperature (°C)	$Normal_{RMS}$ (V)	Temperature (°C)	$Warm_{RMS}$ (V)
1	-18	0.0048	2	0.0279	22	0.0252
2	-17	0.0112	3	0.0168	23	0.0320
3	-16	0.0056	4	0.0079	24	0.0371
4	-15	0.0058	5	0.0107	25	0.0312
5	-14	0.0057	6	0.0089	26	0.0291
6	-13	0.0047	7	0.0112	27	0.0131
7	-12	0.0051	8	0.0140	27	0.0310
8	-11	0.0039	9	0.0120	29	0.0246
9	-10	0.0117	10	0.0100	30	0.0562
10	-9	0.0079	11	0.0176	31	0.0293
11	-8	0.0046	12	0.0223	32	0.0286
12	-7	0.0057	13	0.0190	33	0.0291
13	-6	0.0057	14	0.0159	34	0.0280
14	-5	0.0056	15	0.0144	35	0.0286
15	-4	0.0104	16	0.0197	36	0.0258
16	-3	0.0075	17	0.0250	37	0.0278
17	-2	0.0054	18	0.0103	38	0.0220
18	-1	0.0080	19	0.0310	39	0.0265
19	0	0.0083	20	0.0243	40	0.0441
20	1	0.0108	21	0.0377	41	0.0302
Median	-8.5	0.0057	11.5	0.01635	31.5	0.02885
Interquartile range	-18~1	0.0039~0.0117	2~21	0.0079~0.0377	22~41	0.0131~0.0562

TABLE 2. The meaning of parameters A_1 A_2 A_3 A_4 A_5 and system operation time analysis.

Operation	Triangular calculation	Table look-up	Interpolation	Floating-point multiplication	Floating-point addition
Variable	A_1	A_2	A_3	A_4	A_5
Operation time of CPU	3.546	0.02203	0.02609	0.0226	0.0246
Normalized	355	2.2	2.6	2.2	2.5

differently under different environmental conditions. Based on this feature, the subsection process goes forward. The test environment is divided into cold test (−18°∼1°), normal test (2°∼21°) and warm test(22°∼41°) which is shown in Tab.1.

Fig.11 shows the temperature drift values for all subjects from each test when plotted against their corresponding temperature value. In the first place, all the drift points for the cold test are below 0.0117 V. Points for the normal test are more scattered over a wider range of 0.0079 – 0.0337 V relative to cold test. For the warm test, all the points lie between a highest range of 0.0131 – 0.0562 V. Least-squares fitting results in a low, relatively flat fit to cold and warm test, a steeper gradient to normal test.

Pervious researches mostly focus on fast Fourier transform. Further improvement based on the Goertzel algorithm comes forward as a pulse wave signal concentrates in low frequency. By contrast, table look-up combing with interpolation (TLI) presented in this design saves register space as well as reduce processing time prominently. The calculation for the time cost of fast Fourier transformation (FFT) and table look-up combing with interpolation (TLI) has been listed as follows:

$$\begin{aligned} time_{FFT} &= A_1(p_1p_2)^2 + A_4 \times \frac{p_1}{2}\log_2(p_1p_2) \\ &\quad + A_5 \times p_1 \log_2(p_1p_2) \\ time_{TLI} &= 2N \times p_2 \times (A_3 + 4A_2 + 3A_4 + 4A_5) \end{aligned} \quad (16)$$

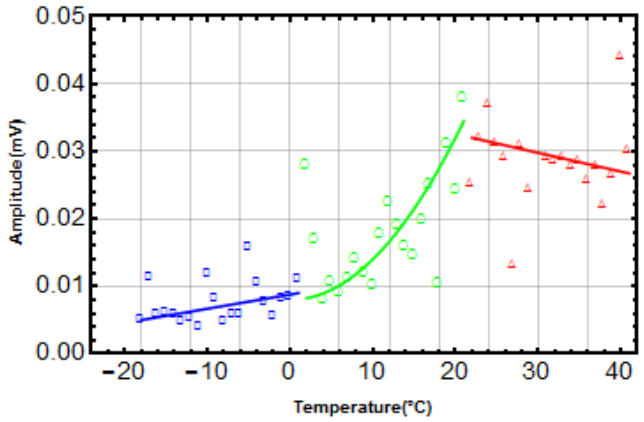

FIGURE 11. **The temperature drift values.**

Tab.2 clearly demonstrates the meaning of parameters A_1 A_2 A_3 A_4 A_5. In order to intuitively test the advantages of the instrument, the processing time when N equals 300 was tested. The processing time of table look-up combing with interpolation (TLI) is 0.19s while fast Fourier transformation (FFT) needs 5.31s. Table look-up combing with interpolation (TLI) increases processing speed by thirty times, as anticipated, enhance the efficiency of the system.

V. CONCLUSION

This paper has presented a non-invasive, high precision and processing speed, multi-parameter pulse analysis system based on the signals collected from the earlobe. It is obvious that the sensitivity of the system is strongly dependent on the sensor of the sampling circuit. Therefore, in the acquisition part of the proposed system, Monte Carlo simulation is utilized. Nonetheless, the sensor has an inherent drawback that cannot be eliminated through the production process improvement. The solution to this problem is calibrating the temperature drift in the different using condition and then carrying on temperature compensation by programming. Aiming to minimize the influence of kinds of noise, the method which can reduce both high frequency noise and baseline drift has been come up in pre-processing section. When the processing steps mentioned above are done, standard pulse wave that will be used to extract health information is obtained. The standard pulse wave is well matched to the simulation results. For the purpose of realizing the processing speed enhancement and reducing the complexity and cost of the hardware circuit, non-linear quantification and looking up table combining with interpolation (TLI) has been presented. In the end part, system test on a random sample of 300 people has been carried out which shows that the testing parameters of this system are extremely accurate. The processing speed is obviously higher than using Fourier algorithm. Through the study, a system which has great advantages in that it can be widely used in practical engineering whether health management instruments or medical measurement device.

REFERENCES

[1] I. Koohi, I. Batkin, V. Z. Groza, S. Shirmohammadi, H. R. Dajani, and S. Ahmad, "Metrological characterization of a method for blood pressure estimation based on arterial lumen area model," *IEEE Trans. Instrum. Meas.*, vol. 66, no. 4, pp. 734–745, Apr. 2017.

[2] E. K. Kim *et al.*, "Brachial-ankle pulse wave velocity as a screen for arterial stiffness: A comparison with cardiac magnetic resonance," *Yonsei Med. J.*, vol. 56, no. 3, pp. 617–624, 2015.

[3] J. Sola, O. Chételat, C. Sartori, Y. Allemann, and S. F. Rimoldi, "Chest pulse-wave velocity: A novel approach to assess arterial stiffness," *IEEE Trans. Biomed. Eng.*, vol. 58, no. 1, pp. 215–223, Jan. 2011.

[4] K. J. Jeon, S.-J. Kim, K. K. Park, J.-W. Kim, and G. Yoon, "Noninvasive total hemoglobin measurement," *J. Biomed. Opt.*, vol. 7, no. 1, pp. 45–50, 2002.

[5] C.-H. Luo, C.-J. Sub, T.-Y. Huanga, and C.-Y. Chung, "Non-invasive holistic health measurements using pulse diagnosis: I. Validation by three-dimensional pulse mapping," *Eur. J. Integr. Med.*, vol. 8, no. 6, pp. 921–925, 2016.

[6] D. Buxi, J. M. Redouté, and M. R. Yuce, "Blood pressure estimation using pulse transit time from bioimpedance and continuous wave radar," *IEEE Trans. Biomed. Eng.*, vol. 64, no. 4, pp. 917–927, Apr. 2017.

[7] H. Hanssen, M. Nussbaumer, C. Moor, M. Cordes, C. Schindler, and A. Schmidt-Trucksass, "Acute effects of interval versus continuous endurance training on pulse wave reflection in healthy young men," *Atherosclerosis*, vol. 238, no. 2, pp. 399–406, 2015.

[8] A. Bongrain *et al.*, "A new technology of ultrathin AlN piezoelectric sensor for pulse wave measurement," *Procedia Eng.*, vol. 120, pp. 459–463, Jan. 2015.

[9] Y. Yamakoshi *et al.*, "A new non-invasive method for measuring blood glucose using instantaneous differential near infrared spectrophotometry," in *Proc. Int. Conf. IEEE Eng. Med. Biol. Soc.*, Aug. 2007, pp. 2964–2967.

[10] M. Nitzan and S. Engelberg, "Three-wavelength technique for the measurement of oxygen saturation in arterial blood and in venous blood," *J. Biomed. Opt.*, vol. 14, no. 2, pp. 24–46, 2009.

[11] E. M. Salido, L. N. Servalli, J. C. Gomez, and C. Verrastro, "Phototransduction early steps model based on Beer–Lambert optical law," *Vis. Res.*, vol. 131, pp. 75–81, Feb. 2017.

[12] V. Ralevic and W. R. Dunn, "Purinergic transmission in blood vessels," *Auton. Neurosci.*, vol. 191, pp. 48–66, Sep. 2015.

[13] D. Shao *et al.*, "Noncontact monitoring of blood oxygen saturation using camera and dual-wavelength imaging system," *IEEE Trans. Biomed Eng.*, vol. 63, no. 6, pp. 1091–1098, Jun. 2016.

[14] Y.-D. Lin, Y.-H. Chien, and Y.-S. Chen, "Wavelet-based embedded algorithm for respiratory rate estimation from PPG signal," *Biomed. Signal Process. Control*, vol. 36, pp. 138–145, Jul. 2017.

[15] T. Y. Abay and P. A. Kyriacou, "Reflectance photoplethysmography as noninvasive monitoring of tissue blood perfusion," *IEEE Trans. Biomed. Eng.*, vol. 62, no. 9, pp. 2187–2195, Sep. 2015.

[16] X. Cui, S. Bray, and A. L. Reiss, "Functional near infrared spectroscopy (NIRS) signal improvement based on negative correlation between oxygenated and deoxygenated hemoglobin dynamics," *Neuroimage*, vol. 49, no. 4, pp. 3039–3046, 2010.

[17] K. Takazawa *et al.*, "Assessment of vasoactive agents and vascular aging by the second derivative of photoplethysmogram waveform," *Hypertension*, vol. 32, no. 2, pp. 365–370, 1998.

[18] Y.-J. An, B.-H. Kim, G.-H. Yun, S.-W. Kim, S.-B. Hong, and J.-G. Yook, "Flexible non-constrained RF wrist pulse detection sensor based on array resonators," *IEEE Trans. Biomed. Circuits Syst.*, vol. 10, no. 2, pp. 300–308, Apr. 2016.

[19] C.-P. Chua, G. Mcdarby, and C. Heneghan, "Combined electrocardiogram and photoplethysmogram measurements as an indicator of objective sleepiness," *Physiol. Meas.*, vol. 29, no. 8, p. 857, 2008.

[20] S. Wassertheurer *et al.*, "A new oscillometric method for pulse wave analysis: Comparison with a common tonometric method," *J. Hum. Hypertens.*, vol. 24, no. 8, pp. 498–504, 2010.

[21] R. G. Haahr *et al.*, "An electronic patch for wearable health monitoring by reflectance pulse oximetry," *IEEE Trans. Biomed. Circuits Syst.*, vol. 6, no. 1, pp. 45–53, Feb. 2012.

[22] M. Tavakoli, L. Turicchia, and R. Sarpeshkar, "An ultra-low-power pulse oximeter implemented with an energy-efficient transimpedance amplifier," *IEEE Trans. Biomed. Circuits Syst.*, vol. 4, no. 1, pp. 27–38, Feb. 2010.

IEEE Journal of Translational Engineering in Health and Medicine

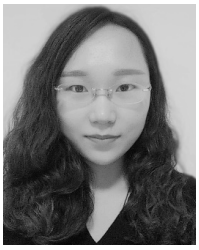

YUNHUI JIANG did an Internship at the Institute of Semiconductors, Chinese Academy of Sciences, in 2016. She is currently pursuing the bachelor's degree with Yancheng Teachers University. She received the National Scholarship of China twice in 2015 and 2017. Her main research interests are medical information processing and electronic system development.

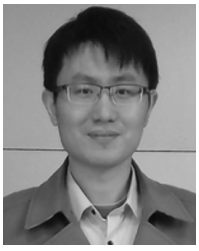

JIAN TANG received the B.A. degree in microelectronics from Peking University and the Ph.D. degree in microelectronics and solid-state electronics from the Institute of Semiconductors, Chinese Academy of Sciences. He is currently an Associate Professor with Yancheng Teachers University. His main research interests are sensor-based systems and medical information processing.

XIAOLIANG WANG received the B.A. degree from Northwest University, China, and the Ph.D. degree from the Xi'an Institute of Optics and Precision Mechanics, Chinese Academy of Sciences. He is currently a Program Director with the Institute of Semiconductors, Chinese Academy of Sciences. He is the Director of the Chinese Institute of Electronics and also a Professor with the University of Chinese Academy of Sciences. His main research interests are GaN-based systems and medical information processing.

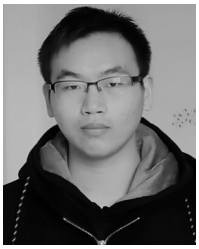

CHAO SHEN is currently pursuing the bachelor's degree with the Yancheng Teachers University of China. He is adept at video editing and has achieved excellent results in relevant competitions. His main research interests are machine learning in the field of artificial intelligence and medical information processing. He received scholarships in 2016 and 2017. He received the title of Excellent Volunteer and Outstanding Student Cadre on Campus in 2014.